Int. J. Electrochem. Sci., 15**(2020)** 5373 – 5384, doi: 10.20964/2020.06.45

International Journal of
ELECTROCHEMICAL
SCIENCE
www.electrochemsci.org

Role of Br^- on the Formation of a Bismuth Nanodendrite Structure and Its Use as an Electrochemical Sensor for Heavy Metal Detection

Nguyen Hoang Anh[1], *Pham Khac Duy*[2], *Pham Thi Hai Yen*[1], *Le Quoc Hung*[1], *Pham Hong Phong*[1], *Vu Thi Thu Ha*[1,3,*], *Hoeil Chung*[2,*]

[1] Institute of Chemistry, Vietnam Academy of Science and Technology (VAST), 18 Hoang Quoc Viet, Cau Giay, Hanoi, Vietnam
[2] Department of Chemistry and Institute for Materials Design, College of Natural Sciences, Hanyang University, Seoul, 04763, Korea
[3] University of Science and Technology of Hanoi, Vietnam Academy of Science and Technology (VAST), 18 Hoang Quoc Viet, Cau Giay, Hanoi, Vietnam
[*]E-mail: havt@ich.vast.vn, hoeil@hanyang.ac.kr

Received: 9 February 2020/ *Accepted:* 23 March 2020 / *Published:* 10 May 2020

Bismuth nanodendrites (BiNDs) were fabricated by simple, one-step electrodeposition of Bi and employed for simultaneous detection of Cd^{2+} and Pb^{2+} in water samples. To construct reliable BiNDs on a glassy carbon electrode (BiND@GCE) without agglomeration and structural imperfections, Br^- was used as a co-reagent to prohibit agglomeration of Bi. The simultaneously generated hydrogen bubbles from H_2 evolution at the surface during Bi deposition could largely cover potential nucleation sites and subsequently suppress the fast agglomeration of Bi. Britton-Robinson buffer, which allowed the formation of $BiPO_4$ on the surface, was used to ensure the stability of the BiNDs during the electrochemical scans. When BiND@GCE was used to measure Cd^{2+} and Pb^{2+} concentrations in aqueous standard samples (concentration range: 2–270 ppb), the achieved limits of detection (LODs) were 0.09 (Cd^{2+}) and 0.05 (Pb^{2+}) ppb. Next, when real field samples obtained from the river and sea were analyzed with BiND@GCE and the subsequent results were compared with those obtained using inductively coupled plasma mass spectrometry, the measurements were accurate, with a recovery range of 89.9-99.3%. Overall, BiNDs represent a versatile electrochemical sensing material, especially for on-site water analysis, with low cost and no serious concern of environmental contamination.

1. INTRODUCTION

Bismuth (Bi) was first adopted as a potential material for electrochemical sensing by Joseph Wang in 2000 [1] and was demonstrated as a promising alternative to a mercury drop electrode because it provided a wide potential window and a high signal-to-noise ratio. Moreover, this element is nontoxic and inexpensive; therefore, it is readily employable for the electrochemical detection of various analytes.

Conventionally, a Bi-based sensor uses a Bi nanostructure that provides a large active surface area for improving the sensitivity of electrochemical measurements. Although Bi nanoparticles and nanostructured Bi films were previously demonstrated as sensitive electrochemical sensors for various analytes (see Table 1), a more effective Bi nanostructure to ensure high sensitivity is in great demand. Nonetheless, the exploration of diverse Bi nanostructures has been relatively sluggish. As an effort to search for new Bi-based nanostructures, in this publication, we fabricated Bi nanodendrites (BiNDs) via simple one-step electrodeposition of Bi and evaluated the subsequent analytical performance for the simultaneous electrochemical detection of Cd^{2+} and Pb^{2+} in water samples. As previously reported, a BiND resembles a pine needle and possesses hierarchical terraces along a central column [2, 3], so it is able to provide a large electrochemically active surface area. Agglomeration and structural imperfections are major challenges in the construction of reliable BiNDs. To avoid these problems, one-step electrodeposition of Bi was designed to build BiNDs on a glassy carbon electrode (GCE) (referred to as BiND@GCE), and the bromide ion (Br^-) was used as a co-reagent during electrodeposition to prohibit agglomeration of Bi. An optimal Br^- concentration yielding optimal BiNDs was explored, and the structures of the built BiNDs were examined using relevant analytical tools.

In previous measurements using Bi-based electrodes, an acetate electrolyte was usually chosen because it provided a low background current with a good signal-to-noise ratio. However, Bi can be easily oxidized under this condition due to the existence of multiple oxidation states (Bi^+, Bi^{2+}, Bi^{3+}) [4], so the stability of the Bi ion was the most concerning issue. Therefore, an alternative electrolyte able to maintain the stability of the BiND structure during the electrochemical scan was searched. For this purpose, Britton-Robinson (BR) buffer was uniquely qualified because of its ability to form stable $BiPO_4$ [5], which would prohibit oxidation of Bi during measurements.

Next, under the determined conditions, BiND@GCE was used to measure the concentrations of both Cd^{2+} and Pb^{2+} in aqueous standard samples, and the resulting linearity and LOD were evaluated. Finally, the Cd^{2+} and Pb^{2+} concentrations in real field samples collected from a river and sea were determined using BiND@GCE, and the resulting determinations were compared to measured concentrations using inductively coupled plasma mass spectrometry (ICP-MS).

2. EXPERIMENTAL

2.1. Preparation of BiND@GCE

A GCE (Metrohm) with a diameter of 3 mm was used as a platform to construct BiNDs. The surface of the GCE was polished to a mirror finish and then sonicated with acetone to remove potential organic contaminants before initiation of electrodeposition. The GCE was immersed in a solution containing 1 mM $Bi_5O(OH)_9(NO_3)_4$, 0.1 M HCl, and KBr (Merck, Germany) as a co-reagent, and a current of -10 mA was applied to the GCE to chronopotentiometrically form BiNDs on the surface. During the application of current, the potential was maintained from -2.8 ~ -2.6 V. KBr concentrations of 0.05, 0.1, and 0.15 M were used to obtain BiNDs with an optimal structure, and the deposition time lasted 90 s in each case.

For comparison, a Bi film was constructed on a GCE (BiF@GCE) according to the method reported in a previous publication [6]. Briefly, a GCE was immersed in a solution containing 20 mg/L Bi^{3+} and 40

mg/L NaBr (an auxiliary ligand) in 0.1 M acetate buffer, and a current of -0.1 mA (vs Ag/AgCl) was applied over 250 s. BiND@GCE and BiF@GCE were thoroughly rinsed and stored in a desiccator before use. Scanning electron microscopy (SEM) images of the fabricated BiNDs were acquired using a Hitachi S-4800 SEM instrument. Transmission electron microscopy (TEM) images and energy dispersive X-ray (EDX) spectra were obtained using a JEM-2100F system (JEM-2100F, JEOL, Japan) with an accelerating voltage of 200 kV. ICP-MS (Perkin Elmer, Elan 9000) was used to determine the concentrations of Cd^{2+} and Pb^{2+} in the real field samples. The RF power, nebulizer gas flow, lens voltage, dwell time, and integration time were 1200 W, 0.71~0.80 L/min, 6.0~7.0 V, 100 ms, and 2000 ms, respectively.

2.2. Sample preparation and electrochemical measurements

Samples containing Cd^{2+} and Pb^{2+} at varying concentrations (2–270 ppb) were prepared by diluting 1000 ppm stock solutions (Merck). Each sample was prepared immediately before the electrochemical measurement. A BR buffer solution (pH = 3) containing 0.04 M H_3PO_4, 0.04 M CH_3COOH, and 0.04 M H_3BO_3 was used as the supporting electrolyte for all electrochemical measurements. Acetate buffer (0.04 M, pH = 3) was employed for comparison. Double-distilled water (WSC/4D, Hamilton Laboratory Glass, UK) was used for the preparation of all the samples in this study.

Voltammograms of the samples (20 mL) were recorded by differential pulse anodic stripping voltammetry (DPASV). Initially, each sample was preconcentrated at -1.0 V for 300 s with magnetic stirring (350 rpm) and equilibrated for 10 s. Then, a corresponding stripping voltammogram was recorded in the scan range from -1.0 to -0.3 V with a pulse height of 70 mV and pulse width of 40 ms. All electrochemical measurements were carried out using a homemade computerized polarographic analyzer (CPAiocHH5, Institute of Chemistry, VAST, Vietnam) at room temperature (25 ± 1 °C). It was equipped with 12 byte analog-digital and digital-analog converters, and the signal was amplified by two operational amplifiers with an active filter. Noise was reduced by the active filter. Overall, the system provided a current resolution down to 0.008 nA. The electrochemical cell was composed of a conventional three-electrode system: Ag/AgCl reference electrode, Pt counter electrode, and BiND@GCE (working electrode).

3. RESULTS AND DISCUSSION

3.1. Construction of BiNDs on the GCE and characterization of the BiND structure

As previously reported, incorporation of negative halide ions during electrodeposition of metal has been helpful to construct the desired nanostructure and avoid undesired agglomeration [2, 7]. Similarly, Br^- was employed as a co-reagent in electrodeposition in this study, and its optimal concentration for yielding the desired BiND structure was explored. Figure 1 shows SEM images of BiNDs constructed with Br^- concentrations of 0, 0.05, 0.10, and 0.15 M. The duration of electrodeposition in all cases was 90 s, which was the optimal condition found in our previous report

[8]. In the absence of Br^-, large, oval-shaped aggregates were clearly seen in the SEM image, while BiNDs were simultaneously formed (Fig. 1 (a)).

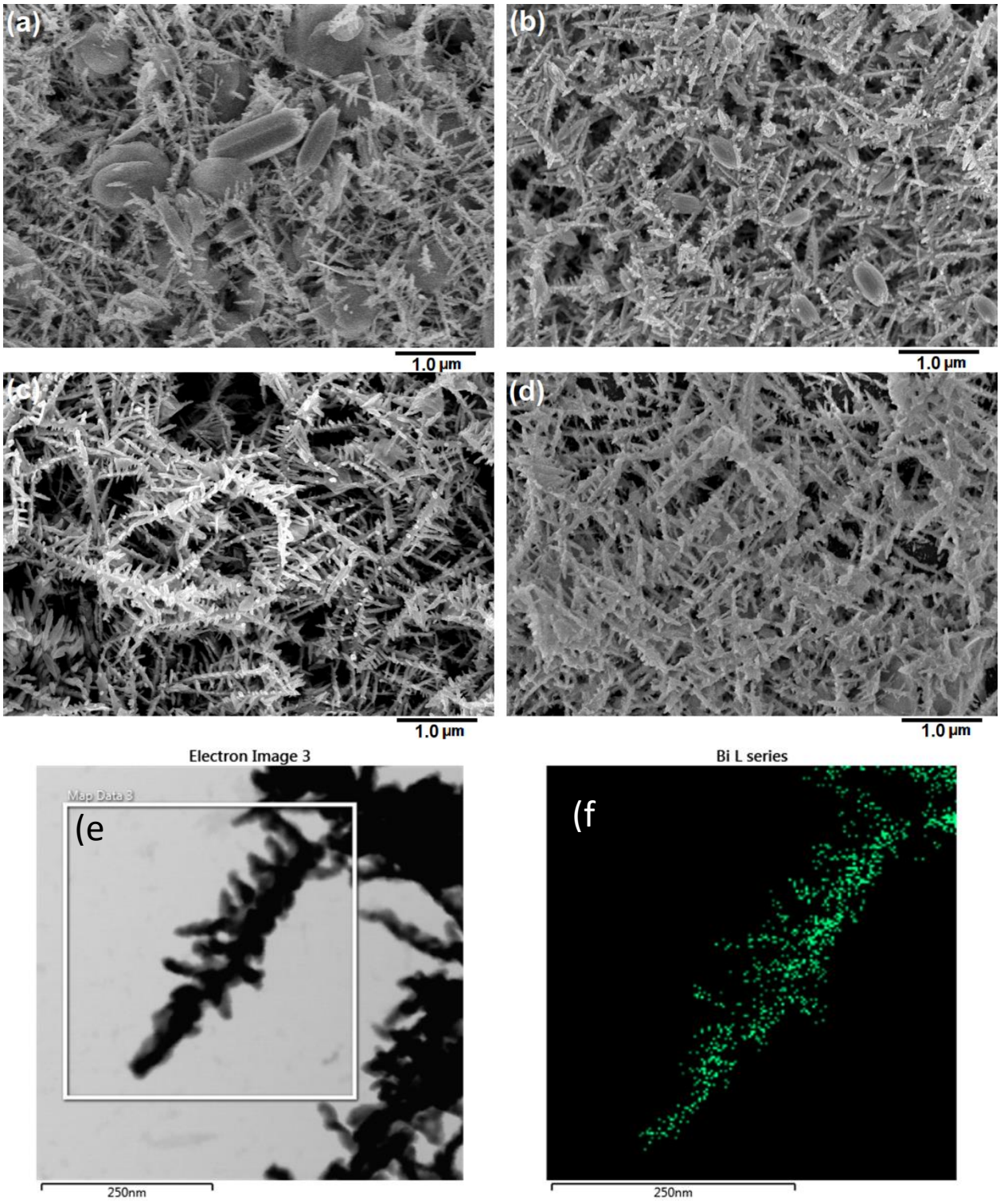

Figure 1. SEM images of BiNDs constructed with Br^- concentrations of (a) 0, (b) 0.05, (c) 0.1, and (d) 0.15 M and TEM images of the top part of a single Bi nanodendrite (e) and the corresponding elemental mapping of Bi (f) in the branches of the nanodendrite structure. The duration of electrodeposition in all cases was 90 s.

An increase in the Br^- concentration (0.05 M) decreased the size of the oval aggregates (Fig. 1 (b)), and a further concentration increase (0.10 M) clearly resulted in the formation of BiNDs without aggregates (Fig. 1 (c)). When the Br^- concentration was greater than 0.10 M, the edges and terraces of the BiNDs were blunt and lost their sharpness (Fig. 1 (d)). These results confirm that the use of Br^- at optimal concentrations was necessary to form the BiND structure without unwanted aggregation or a blunt structure. TEM images of the top part of a single Bi nanodendrite are also presented ((e) and (f)).

The role of Br^- in the formation of nanodendrite structures can be explained based on three previous reports [9-11]. In these studies, the complexation of Bi with Br^- improved the deposition of Bi onto carbon substrate electrodes, resulting in the growth of Bi crystals on a GCE in the presence of Br^- in the plating solution. Additionally, two competitive reactions of Bi^{3+} reduction and H_2 evolution generating H_2 bubbles simultaneously occurred at the surface. The generated hydrogen bubbles could largely cover the potential nucleation sites and subsequently suppress the fast agglomeration of Bi. Therefore, these two sources are responsible for the growth of Bi nanodendrites into rather agglomerated structures.

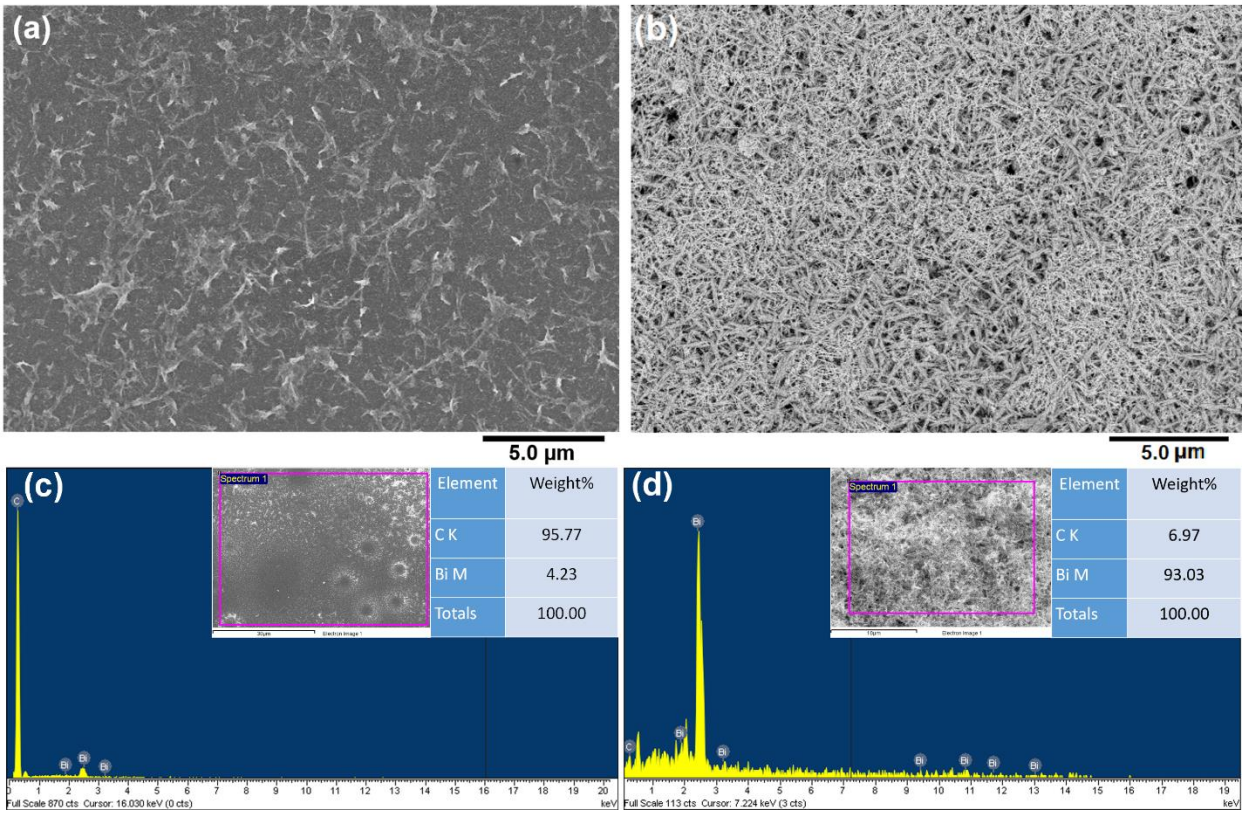

Figure 2. SEM images of the surface of BiND@GCE after 10 electrochemical scans over the range from -0.9 to -0.3 V in acetate (a) and BR buffer (b) and the corresponding EDX spectra ((c) and (d), respectively).

Acetate electrolyte was used in previous measurements with Bi-based electrodes because it provided a low background current with a good signal-to-noise ratio. However, Bi could be easily

oxidized in this environment due to the existence of multiple oxidation states (Bi^{+}, Bi^{2+}, Bi^{3+}) [4], and surface stability was an important concern. To assess stability, BiND@GCE was immersed in acetate buffer, and 10 electrochemical scans were performed consecutively over the range of -0.9 to -0.3 V. The resulting SEM image of the BiNDs was examined, as shown in Figure 2 (a). For comparison, the same test was performed in BR buffer (Fig. 2 (b)). When acetate buffer was used, BiNDs mostly disappeared due to oxidation of Bi (Fig. 2 (a)), and only 4.23% of the BiNDs remained after 10 scans (Fig. 2 (c)), indicating substantial elimination of the nanostructures. A carbon peak was mostly dominant in the corresponding EDX spectrum. Further, when the pH and concentration of acetate buffer were changed to 4.5 and 0.1 M for the same test, respectively, the BiNDs again disappeared after 10 scans (relevant data are not shown). In contrast, 93% of the BiNDs remained when using BR buffer (Fig. 2 (b)), based on analysis of the acquired EDX spectrum (Fig. 2 (d)). This observation confirmed the stability of the BiNDs during the electrochemical scan in BR buffer due to the formation of stable $BiPO_4$. Therefore, BR buffer was solely adopted for subsequent measurements.

3.2. Detection of Cd^{2+} and Pb^{2+} in samples using BiND@GCE

Table 1 summarizes the Bi film-based electrodes and their analytical performance-response range and limit of detection (LOD) in the measurement of Cd^{2+} and Pb^{2+}. In the early stages of use, Bi films were built on various carbon-based platforms, such as glassy carbon [1, 12, 13], carbon paste [14, 15], wax impregnated graphite [13], pencil lead [16], and screen-printed carbon ink [17]. The glassy carbon electrode (GCE) was a preferable choice due to its good durability and low background current [14], but the obtained LODs of Cd^{2+} and Pb^{2+} measurement by using such electrodes were only at the 10 ppb level. In later studies, other materials that were able to improve electrochemical detection performance were incorporated into the Bi film (Table 1), such as polystyrene sulfonate-carbon nanopowder [18], mesoporous carbon [19], active graphene composites [20], carbon nanotubes [21], and ionic liquids [22]. As shown, very low LODs, such as 0.02 and 0.03 ppb, were achieved in cases using Bi/ionic liquid-graphite paste electrodes [23] and Bi-polystyrene sulfonate-carbon nanopowder electrodes [18], respectively. However, the electrodes used in a previous study show disadvantages in terms of complications in the sensor preparation procedures. The proposed BiND@GCE in this study overcomes the previous disadvantages by achieving very LODs in the simultaneous detection of Cd^{2+} and Pb^{2+} (10^{-2} ppb scale) with simple sensor preparation by single-step electrodeposition.

Table 1. Summary of previously reported Bi-based electrodes and their tested range and limit of detection (LOD) in the measurement of Cd^{2+} and Pb^{2+}.

Description of electrode	Range (ppb)	LOD (ppb)	Ref.
Bismuth film/GCE	40-200 (Cd^{2+}), 20-150 (Pb^{2+})	1.1	[1]

Bismuth film/GCE (in situ measurement)	10-70 (Cd^{2+}), 10-100 (Pb^{2+})	-	[12]
Bismuth film/rotating GCE (in situ measurement)	2-18	0.2	[13]
Bismuth film/pencil-lead graphite	2-24	0.3 (Cd^{2+}), 0.4 (Pb^{2+})	[14]
Bismuth film/GCE (in situ measurement)	20-200	0.2 (Cd), 0.8 (Pb^{2+})	[15]
Bismuth film/CPE	20-140 (Pb^{2+})	3.16	[16]
Bismuth bulk electrode	10-200 (Pb^{2+})	3.2	[17]
Bismuth nanoparticle-porous carbon nanocomposite SPE	1-50	1.5 (Cd^{2+}), 2.3 (Pb^{2+})	[23]
Bismuth film/SPE (in situ measurement)	5-50 (Cd^{2+}), 5-60 (Pb^{2+})	1.5 (Cd^{2+}), 0.3 (Pb^{2+})	[24]
Bismuth oxide/SPE	0-12	0.2	[25]
Bismuth nanoparticle/porous CPE	1-100	0.81 (Cd^{2+}), 0.65 (Pb^{2+})	[26]
Bismuth/ionic liquid-graphite paste electrode	0.1-2.8	0.01 (Cd^{2+}), 0.02 (Pb^{2+})	[27]
Pencil-lead bismuth film electrode	5-11 (Cd^{2+}), 20-65 (Pb^{2+})	-	[28]
Bismuth film/GCE	10-40	2.03 (Cd^{2+}), 2.43 (Pb^{2+})	[29]
Nanostructured bismuth film/GCE	20-100	0.4 (Cd), 0.1 (Pb^{2+})	[6]
Bismuth film/GCE	1-170 (Cd^{2+})	0.3	[30]
Bismuth/sol-gel microspheres	1.0-17.0 (Cd^{2+}), 1.8-31.8 (Pb^{2+})	1.4 (Cd^{2+}), 1.2 (Pb^{2+})	[31]
Bismuth film/boron-doped diamond electrode	-	0.35 (Cd^{2+}), 0.34 (Pb^{2+})	[32]
Bismuth-polystyrene sulfonate-carbon nanopowder/SPE	0.5-15	0.012 (Cd^{2+}), 0.029 (Pb^{2+})	[18]
Bismuth film-ordered mesoporous carbon/modified CPE	1-70	0.07 (Cd^{2+}), 0.08 (Pb^{2+})	[19]
Graphene-bismuth nanocomposite film/GCE	1-100	0.18 (Cd^{2+}), 0.11 (Pb^{2+})	[20]
Activated graphene-Nafion bismuth composite film	5-100	0.07 (Cd^{2+}), 0.05 (Pb^{2+})	[33]
Bismuth-reduced graphene oxide/Au electrode	1-120	1.0 (Cd^{2+}), 0.4 (Pb^{2+})	[34]
Bismuth nanoparticle/nanoporous carbon-graphene sheet	26-257 (Cd^{2+}), 12-124 (Pb^{2+})	1.32 (Cd^{2+}), 0.66 (Pb^{2+})	[35]
Bismuth film-polyaniline nanofibers-mesoporous carbon nitride/GCE	5-80	0.7 (Cd^{2+}), 0.2 (Pb^{2+})	[36]
Bismuth-MWCNT-emeraldine based polyaniline-Nafion/GCE	1-50	0.06 (Cd^{2+}), 0.08 (Pb^{2+})	[37]

Bismuth-oxychloride particle-MWCNT composite/GCE	5-50	1.20 (Cd^{2+}), 0.57 (Pb^{2+})	[38]
Bismuth-MWCNT-poly(pyrocatechol violet)/GCE	1-300 (Cd^{2+}), 1-200 (Pb^{2+})	0.2 (Cd^{2+}), 0.4 (Pb^{2+})	[39]
Bismuth-Nafion-ionic liquid-graphene composite/SPE	0.1-100	0.06 (Cd^{2+}), 0.08 (Pb^{2+})	[22]
Bismuth film-mesoporous graphene-Nafion/GCE	2-70 (Cd^{2+}), 0.5-110 (Pb^{2+})	0.5 (Cd^{2+}), 0.1 (Pb^{2+})	[40]
Bismuth-reduced graphene oxide/SPE	10.35-41.40 (Pb^{2+})	1.4 (Pb^{2+})	[41]
Bismuth-Ag nanoparticle-Nafion/SPE	0.5-400 (Cd^{2+}), 0.1-500 (Pb^{2+})	0.5 (Cd^{2+}), 0.1 (Pb^{2+})	[42]
Bismuth nanodendrite/GCE	2-270	0.09 (Cd^{2+}), 0.05 (Pb^{2+})	This work

GCE: glassy carbon electrode CPE: carbon paste electrode
MWCNT: multiwall carbon nanotube SPE: screen-printed electrode

Initially, both BiND@GCE and BiF@GCE were employed to measure a sample with 40 ppb Cd^{2+} and Pb^{2+} for comparison, as shown in Figure 3 (a). The peaks of Cd^{2+} and Pb^{2+} clearly appear at -0.70 and -0.45 V, respectively, and the peak intensities are approximately 5 times higher in the measurement with BiND@GCE. This test confirmed that in comparison with the Bi film structure, the nanodendrite structure, which provided a large surface-to-volume ratio, was effective in enhancing the sensitivity. Figure 3 (b) shows voltammograms of all the samples measured using BiND@GCE. Both the Cd^{2+} and Pb^{2+} peak heights increased with increasing analyte concentration. Figure 3 (c) and (d) shows the response curve generated using the peak height in the measurement of the Cd^{2+} and Pb^{2+} concentrations, respectively. The error bars are based on three measurements using three separately prepared BiND@GCEs. In each case, the variation in peak intensity was linear in the tested concentration range, with R^2 values of 0.987 (Cd^{2+}) and 0.991 (Pb^{2+}). Next, the LOD was calculated based on the response curve in the figure ($LOD = 3.3 \times \frac{SD}{b}$; SD: standard deviation of the ordinate intercept, b: slope of regression line). The LODs were 0.09 and 0.05 ppb for the detection of Cd^{2+} and Pb^{2+}, respectively. Although the achieved sensitivities are not best in comparison with those reported in previous studies (Table 1), they are clearly superior and in a top-level group.

Meanwhile, the allowable LODs for the detection of Cd^{2+} and Pb^{2+} according to WHO guidelines are 3.0 and 10.0 ppb, respectively [43].

The error bars in the response curve correspond to the standard deviations of peak intensities acquired using the three separate sensors. The magnitudes of the error bars are quite small, and the average relative standard deviations (RSDs) in the measurements of Cd^{2+} and Pb^{2+} are 4.6 and 4.1%, respectively, thereby confirming the reproducible formation of Bi-nanodendrites on the GCE. The repeatability was also evaluated by consecutively measuring a sample containing 40 ppb Cd^{2+} and 40 ppb Pb^{2+} ten times using one sensor. No decreases in peak intensities were observed during the scans in

either case, and the resulting RSDs of the Cd^{2+} and Pb^{2+} peak intensities were 2.2 and 2.3%, respectively. This result confirms the superior surface stability of BiND.

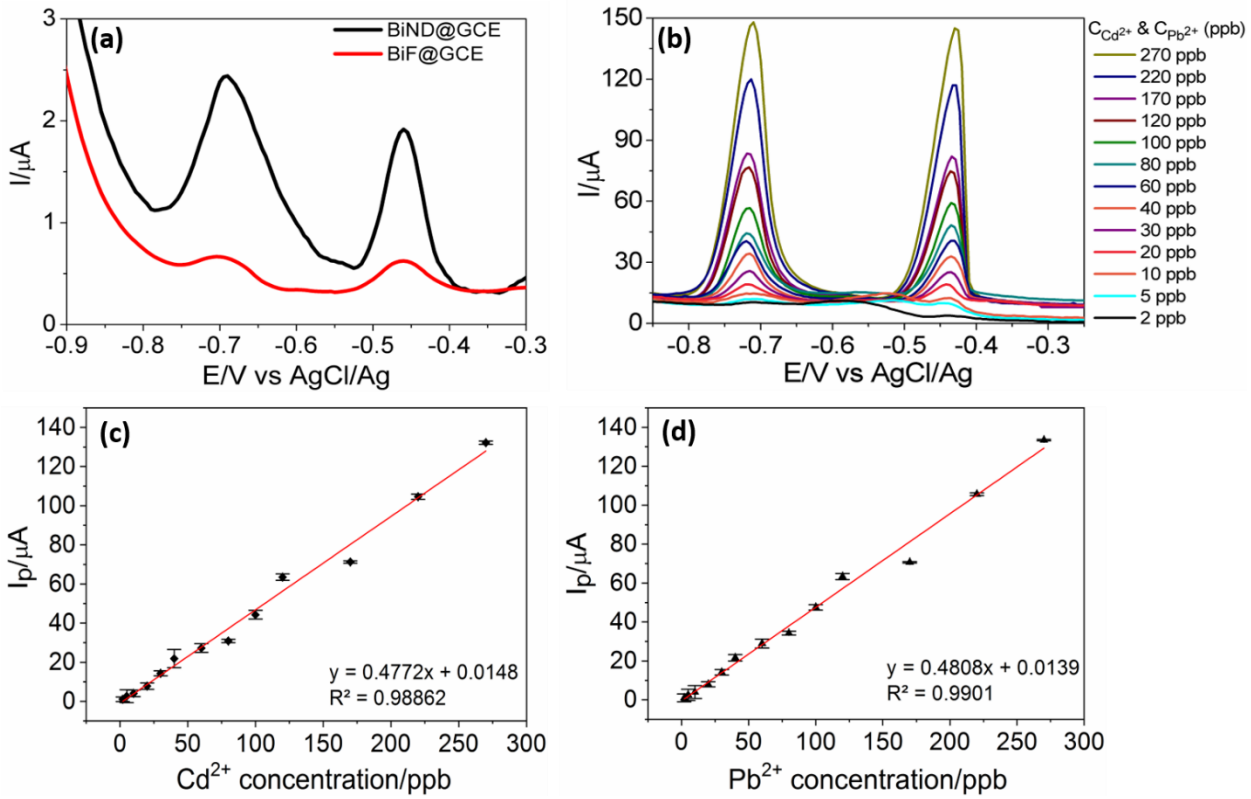

Figure 3. Voltammogram measurements of (a) the 40 ppb Cd^{2+} and Pb^{2+} samples and (b) the standard samples (concentration range: 2–270 ppb). Corresponding response curves in the measurement of (c) Cd^{2+} and (d) Pb^{2+} concentrations are shown.

Table 2. Determined Cd^{2+} and Pb^{2+} concentrations in pure water, sea water, and lake water using BiND@GCE and ICP-MS. The recovery in each case is also shown.

Sample	Added Conc. (ppb)	Cd^{2+} (ppb)			Pb^{2+} (ppb)		
		BiND@GCE	ICP-MS	Recovery	BiND@GCE	ICP-MS	Recovery
Pure water	10	9.9 ± 0.1	10.5	99.3%	9.8 ± 0.3	10.0	98.0%
Sea water	5	4.5 ± 0.1	4.6	89.9%	4.7 ± 0.1	5.0	93.3%
West lake sample	0	Not detected	Not detected	-	2.8 ± 0.23	2.5	-

Finally, BiND@GCE was further used to determine Cd^{2+} and Pb^{2+} concentrations in real samples collected from West Lake (Hanoi, Vietnam) and Cat Ba Island (Hai Phong, Vietnam) according to Standard Methods for Examination of Water and Waste Water (SMEWW) [44]. The samples were filtered through a glass fiber filter to eliminate potential interference from contaminants such as suspended particulates and organic matter. For comparison, an ultrapure water sample containing 10 ppb Cd^{2+} and 10 ppb Pb^{2+} was also measured. In all cases, three replicate measurements were performed. In parallel, the Cd^{2+} and Pb^{2+} concentrations of the same samples were determined using ICP-MS. Table 2 shows the determined Cd^{2+} and Pb^{2+} concentrations in the samples using BiND@GCE as well as ICP-MS and the calculated recoveries. The concentration determinations using BiND@GCE were accurate, with a recovery range of 89.9-99.3%. Therefore, the detection performance of BiND@GCE was comparable to that of ICP-MS.

4. CONCLUSION

The demonstrated easy-to-prepare BiND structure was suitable for sensitive and stable electrochemical measurement of Cd^{2+} and Pb^{2+} in water samples, and the determined analyte concentrations in real field samples using BiND@GCE agreed well with those obtained using ICP-MS. The existence of a Br^- agent at a proper concentration during the BiND preparation process helps to perfect the 3D-BiND hierarchical structure and maximize the BiND surface-active area, which increases the Cd^{2+} and Pb^{2+} detection sensitivity. Furthermore, BiND@GCE, with its low cost and lack of serious concerns regarding environmental contamination, should be employed as an electrochemical sensor for on-site water analysis. A portable analytical system incorporating BiND@GCE with additional sensors is under development for the analysis of field samples. Ongoing research will focus on the incorporation of other materials to improve electrochemical detection, such as graphene oxide in BiND. By doing so, further improvements in the sensitivity and long-term stability of BiND-based sensors can be expected.

ACKNOWLEDGEMENTS
This research is funded by Vietnam National Foundation for Science and Technology Development (NAFOSTED) under grant number 104.06-2016.25 and the Creative Materials Discovery Program on Creative Multilevel Research Center (2015M3D1A1068061) through the National Research Foundation (NRF) of Korea (the Ministry of Science, ICT & Future Planning).

References

1. J. Wang, J. Lu, S. B. Hocevar, P. A. M. Farias, B. Ogorevc, *Anal. Chem.*, 72 (2000) 3218.
2. P. K. Duy, P. T. H. Yen, S. Chun, V. T. T. Ha, H. Chung, *Sens. Actuators*, B,225(2016) 377.
3. V. H. Dang, P. T. H. Yen, N. Q. Giao, P. H. Phong, V. T. T. Ha, P. K. Duy, C. Hoeil, *Electroanalysis*, 30(2018) 2222.
4. A. Yousif, R. M. Jafer, S. Som, M. M. Duvenhage, E. Coetsee, H. C. Swart, *RSC Adv*.,5(2015) 54115.
5. C. Pan, Y. Zhu, *Catal. Sci. Technol*.,5(2015) 3071.

6. T. Zidarič, V. Jovanovski, E. Menart, M. Zorko, M. Kolar, M. Veber, S. B. Hočevar, *Sens. Actuators*, B, 245(2017) 720.
7. T. N. Huan, T. Ganesh, K. S. Kim, S. Kim, S. H. Han, H. Chung, *Biosens. Bioelectron*., 27(2011) 183.
8. N. H. Anh, P. K. Duy, P. T. H. Yen, V. H. Dang, N. Q. Giao, V. T. T. Ha, Vietnam *J. Chem*.,56(2018) 473.
9. E.A. Hutton, S.B. Hočevar, B. Ogorevc, *Anal. Chim. Acta*, 537(2005) 285.
10. A.R. Rajamani, S. Jothi, M.D. Kumar, S. Srikaanth, M.K. Singh, G. Otero-Irurueta, D. Ramasamy, M. Datta, M. Rangarajan, *J. Phys. Chem*. C,120(2016) 22398.
11. Minli Yang, *J. Mater. Chem*.,21(2011) 3119.
12. J. Wang, J. Lu, Ü. A. Kirgöz, S. B. Hocevar, B. Ogorevc, *Anal. Chim. Acta*, 434(2001) 29.
13. G. Kefala, A. Economou, A. Voulgaropoulos, M. Sofoniou, *Talanta*, 61(2003) 603.
14. D. Demetriades, A. Economou, A. Voulgaropoulos, *Anal. Chim. Acta*, 519(2004) 167.
15. S. B. Hocevar, J. Wang, R. P. Deo, B. Ogorevc, *Electroanalysis*, 14(2002) 112.
16. G. -U. Flechsig, O. Korbout, S. B. Hocevar, S. Thongngamdee, B. Ogorevc, P. Gründler, J. Wang, *Electroanalysis,* 14(2002) 192.
17. R. Pauliukaitė, S. B. Hočevar, B. Ogorevc, J. Wang, *Electroanalysis*, 16(2004) 719.
18. R. María-Hormigos, M. J. Gismera, J. R. Procopio, M. T. Sevilla, *J. Electroanal. Chem*.,767(2016) 114.
19. G. Zhao, H. Wang, G. Liu, Z. Wang, *Electroanalysis,*29(2017) 497.
20. S. Lee, S. -K. Park, E. Choi, Y. Piao, *J. Electroanal. Chem*., 766(2016) 120.
21. G. Zhao, H. Wang, G. Liu, *RSC Adv*., 8(2018) 5079.
22. S. Chaiyo, E. Mehmeti, K. Žagar, W. Siangproh, O. Chailapakul, K. Kalcher, *Anal. Chim. Acta*, 918(2016) 26.
23. P. Niu, C. Fernández-Sánchez, M. Gich, C. Navarro-Hernández, P. Fanjul-Bolado, A. Roig, *Microchim. Acta*, 183(2016) 617.
24. N. Colozza, M. F. Gravina, L. Amendola, M. Rosati, D. E. Akretche, D. Moscone, F. Arduini, *Sci. Total Environ.,* 584-585(2017) 692.
25. D. Riman, D. Jirovsky, J. Hrbac, M. I. Prodromidis, *Electrochem. Commun*.,50(2015) 20.
26. P. Niu, C. Fernández-Sánchez, M. Gich, C. Ayora, A. Roig, *Electrochim. Acta*, 165(2015) 155.
27. X. Zhang, Y. Zhang, D. Ding, J. Zhao, J. Liu, W. Yang, K. Qu, *Microchem. J*., 126(2016) 280.
28. G. D. Pierini, M. F. Pistonesi, M. S. D. Nezio, M. E. Centurión, *Microchem. J*., 125(2016) 266.
29. C. L. Jost, L. M. Martos, L. Ferraz, P. C. Nascimento, *Electroanalysis*, 28(2016) 287.
30. G. Zhao, H. Wang, G. Liu, Z. Wang, *Sens. Actuators*, B,235(2016) 67.
31. P. A. Dimovasilis, M. I. Prodromidis, *Anal. Lett*.,49(2016) 979.
32. C. W. Foster, A. P. Souza, J. P. Metters, M. Bertotti, C. E. Banks*, Analyst*,140(2015) 7598.
33. S. Lee, S. Bong, J. Ha, M. Kwak, S. -K. Park, Y. Piao, *Sens. Actuators*, B,215(2015) 62.
34. X. Xuan, M. F. Hossain, J. Y. Park, *Sci. Rep*.,6(2016) 33125.
35. L. Cui, J. Wu, H. Ju, *Chem. - Eur.J*. 21(2015) 11525.
36. C. Zhang, Y. Zhou, L. Tang, G. Zeng, J. Zhang, B. Peng, X. Xie, C. Lai, B. Long, J. Zhu, *Nanomaterials*,6(2016) 1.
37. G. Zhao, Y. Yin, H. Wang, G. Liu, Z. Wang, *Electrochim. Acta*, 220(2016) 267.
38. S. Cerovac, V. Guzsvany, Z. Konya, A. M. Ashrafi, I. Švancara, S. Rončević, Á. Kukovecz, B. Dalmacija, K. Vytřas, *Talanta*,134(2015) 640.
39. M. A. Chamjangali, H. Kouhestani, F. Masdarolomoor, H. Daneshinejad, *Sens. Actuators*, B, 216(2015) 384.
40. L. Xiao, B. Wang, L. Ji, F. Wang, Q. Yuan, G. Hu, A. Dong, W. Gan, *Electrochim. Acta*,222(2016) 1371.
41. X. Hu, D. Pan, M. Lin, H. Han, F. Li, *ECS Electrochem. Lett*.,4(2015) H43.
42. J. Mettakoonpitak, J. Mehaffy, J. Volckens, C. S. Henry, *Electroanalysis*,29(2017) 880.

43. Guidelines for drinking-water quality, World Health Organization, fourth edition (2011) 564.
44. E. W. Rice, R. B. Baird, A. D. Eaton, Standard Methods for the Examination of Water and Wastewater, 23rd ed., American Water Works Association (2017) 4.